Electronic Supplementary Information: Insights into the photoprotection mechanism of the UV filter homosalate

Emily L. Holt,‡[a,b] Konstantina M. Krokidi,‡[a] Matthew A. P. Turner,‡[a,b]
Piyush Mishra,[c] Timothy S. Zwier,[c] Natércia d. N. Rodrigues*[a] and Vasilios G. Stavros*[a]

[a] *Department of Chemistry, University of Warwick, Gibbet Hill Road, Coventry, CV4 7AL, United Kingdom*

[b] *Molecular Analytical Science Centre for Doctoral Training, Senate House, University of Warwick, Coventry, CV4 7AL, United Kingdom*

[c] *Department of Chemistry, Purdue University, West Lafayette, Indiana 47907-2084, United States*

* *To whom correspondence should be addressed. E-mail: v.stavros@warwick.ac.uk, or n.das-neves-rodrigues@warwick.ac.uk*

‡These authors contributed equally to this work.

Contents

List of Figures

List of Tables

S1 Supplementary methods

S1.1 Gas-phase experiments

S1.1.1 Power dependence measurements

The TR-IY signal dependence on both the pump and probe laser powers was evaluated to ensure single-photon-induced photodynamics take place under the current experimental conditions. Firstly, TR-IY transients were collected at three different values of laser power; the logarithm of transient subtracted signal (raw signal minus background signal, *i.e.* pump-only, probe-only and background noise) with respect to the logarithmic value of power for each time delay (log(signal) *vs.* log(power)) is then plotted and finally fit using a linear function using least squares regression. The gradient of this fit provides us with the physical information regarding the signal power dependence — a gradient of 1 (within error) is taken to be indicative of single-photon-induced dynamics. In Fig. S1, an exemplar power study plot is shown for photoexcitation at $\lambda_{pump} = 305$ nm ($\lambda_{probe} = 200$ nm) and at $\Delta t = 0$. The error of the gradient is the standard error for the parameter,

given by the following equation:

$$\frac{b}{\sqrt{n-2}}\sqrt{\frac{1}{r^2}-1} \tag{S1}$$

where b is the fitted gradient from the least squares regression analysis undertaken, n is the number of datapoints on the line, and r is the value of the Pearson correlation coefficient[5] for the fitted data.

Similar power dependence studies were carried out for other pump wavelengths, with similar results (not shown). The error bars shown in Fig. S1 represent two standard deviations from the average data point, which was collected from four consecutive scans. The large error associated with each data point on these plots is a reflection of the low signal-to-noise ratio of these experiments, a consequence of the small pump-probe signal (in comparison to the pump alone and probe alone signals). Albeit inconclusive, the linear fit to these data, as presented in Fig. S1, seems to suggest that the feature associated with τ_1 may be linearly dependent on pump power, which would be indicative of single-photon pump-initiated photodynamics via S_1. We also note here that the large amplitude of the feature from which these data were extracted (particularly noticeable in Fig. 3(c) in the main manuscript) is likely to have a considerable contribution from probe-initiated reverse dynamics, considering the high absorption cross section of our 200 nm probe.

S1.1.2 Kinetic fit

We fit our TR-IY data for the homosalate (HMS) parent ion (HMS^+) transients using a multi-parameter function that can be analytically described as follows:

$$S(t) = g(t) * \sum_{i=0}^{n} A_i \mathrm{e}^{-\frac{t}{\tau_i}} H(t) + \text{offset} \tag{S2}$$

Equation S2 describes the convolution of a Gaussian function $g(t)$ (corresponding to the instrument response function, see below) with a sum of exponential decay functions starting at time zero ($\Delta t = 0$). A_i is then the amplitude of the i-th decay, τ_i the time constant corresponding to the i-th decay and $H(t)$ is a step function defined in Equation S3.

$$H(t) = \begin{cases} 0 & \text{if } t < 0 \\ 1 & \text{if } t \geq 0 \end{cases} \tag{S3}$$

This kinetic fit assumes parallel excited state decay pathways, *i.e.* it assumes that all dynamics begin at $\Delta t = 0$.

S1.1.3 Instrument response function and time zero $\Delta t = 0$

As mentioned in the main manuscript, the instrument response function (IRF) defines the time resolution of our time-resolved measurements. In order to estimate the IRF, TR-IY measurements of Xenon (Xe) were performed, following $2 + 1$ non-resonant ionization (see Fig. S2 for one such measurement, for $\lambda_{\text{pump}} = 330$ nm). The resulting transient, which consists of the cross-correlation between the pump and probe laser pulses, was fit with a Gaussian function; the full width at half maximum (FWHM) of this Gaussian fit, which was determined to be $\sim$ 170 fs, was taken to be our IRF.

S1.1.4 Dispersed fluorescence and fluorescence lifetime

Fig. S3a shows the dispersed fluorescence spectrum of HMS which was obtained following the methodology described in the main paper. Briefly, the laser wavelength was fixed to be resonant with selected transitions in the excitation spectrum and the resulting fluorescence was then dispersed with a grating and collected by an intensified CCD. Upon photoexcitation to the $S_1(v = 0)$ origin of HMS, the resulting dispersed fluorescence spectrum reveals a large Stokes shift of ~ 5800 cm^{-1} or 0.72 eV (see Fig. S3a).

Fluorescence lifetime traces were also recorded by exciting select transitions and directly recording the time profile of the fluorescence signal from the photomultiplier tube on the digital oscilloscope. The gas-phase fluorescence lifetimes of HMS were extracted from the resulting transients following the same method described in section 1.2, using in this case an instrument response of 8 ns. Fig. S3b shows one example of such fluorescence lifetimes measurements, for which excitation was to the $S_1(v = 0)$ of HMS; a fluorescence lifetime of 12.7 ± 0.2 ns was extracted from this fit.

S1.2 Experiments in solution

S1.2.1 Fitting procedure

The spectra collected with our transient electronic absorption spectroscopy (TEAS) setup, further described in the main paper, are chirped, *i.e.* $\Delta t = 0$ is different for each probe wavelength, due to group velocity dispersion (GVD) artefacts.[6] To account for this chirp effect, a third order polynomial is included within the fitting algorithm within the Glotaran software package.[4] This package also convolutes the Gaussian IRF (see Section S1.2.2) with exponential functions to extract the fitted lifetimes (τ_n) for the parallel kinetic model used for this data. In the false colour heat maps and corresponding heat maps presented in the main manuscript and this ESI, the chirp is corrected using the KOALA package.[7]

S1.2.2 Instrument response functions

The IRF for our TEAS setup is determined by evaluating solvent-only responses at given probe wavelengths. The resulting transients were fitted with a Gaussian function, given by Eq. S4. In this equation, A denotes the peak amplitude of the fitted curve, t_0 is the fitted time zero, indicating the centre of the curve, and σ is the standard deviation of the curve. The fits attained using Eq. S4 are shown in Fig. S4.

$$f(t) = A \exp\left(-\frac{t - t_0}{2\sigma^2}\right) + \text{offset} \tag{S4}$$

To convert from the fitted standard deviation to the full width half maximum (FWHM), which is the quoted IRF, a scaling factor of $2\sqrt{2\ln 2}$ was applied to the standard deviation σ. After application of this scaling factor, the extracted IRF lifetimes are $\sim$ 80 fs in acetonitrile, $\sim$ 65 fs in ethanol and $\sim$ 55 fs in cyclohexane.

S1.2.3 Power dependence measurements

Power dependence measurements were taken for each solution of HMS and ethylhexyl salicylate (EHS) in all three solvents: ethanol, acetonitrile and cyclohexane, to ensure a linear dependence on power across all spectral features of the TAS and exclude the possibility of multiphoton transitions, following the relation (log(Signal) *vs.* log(Power)). A gradient of 1 (within error) is suggestive of single photon mediated photodynamics. The power of the pump wavelength was varied for each set of measurements by reducing the output of the TOPAS-C. At each power, 20 datasets were taken and subsequently averaged.

Slices of the transients were taken in the wavelength domain where significant spectral features occur, then the slices were smoothed by using an integration window of $\pm$ 5 nm. The outcome of this power dependence study is shown in Fig. S5 for HMS in ethanol and Fig. S6 for EHS in ethanol. In each case, the error of the gradient is the standard error for the parameter, given by Eq. S1. The values of r that have been substituted into Eq. S1 to attain the gradient standard error presented in Figs. S5 and S6 are as follows:

Fig. S5: (a) 0.962, (b) 0.989, (c) 0.961

Fig. S6: (a) 0.991, (b) 0.993, (c) 0.996

To calculate the error bars in each case, all 20 scans taken at each power were averaged together, and alongside the mean value for each datapoint ($\bar{x}$), the standard deviation (σ) was also recorded. The standard deviation at each single wavelength was then summed across the integrated wavelength region to account for error propagation. The error bars presented in Figs. S5 and S6 are thus equivalent to $\log(\bar{x} \pm 2\sigma)$.

S1.2.4 Fluorescence of homosalate

Emission spectra were measured for HMS in each of three solvents: acetonitrile, ethanol and cyclohexane. Solutions were prepared to a concentration of ~ 10 μM and the path length for spectrum acquisition was 10 mm. The emission spectra were collected using a Horiba Fluorolog-3 instrument; the excitation wavelength was chosen to be the $\lambda_{\max}$ of each solution, 306 nm in acetonitrile, 307 nm in ethanol and 309 nm in cyclohexane, which were produced by a Xenon arc lamp with a slit width of 5 nm.

Fluorescence lifetimes for the three solutions of HMS were also determined. The same samples as the fluorescence measurements above were used to assess the lifetimes, and a 1 cm path length quartz fluorescence cuvette was used. Instead of a Xe arc lamp, the excitation source was a NanoLED with a central wavelength of 318 nm. An exponential decay function was fitted to the fluorescence signal *vs.* time transients to extract the respective fluorescence lifetimes, which were found to be within the instrument response of 1.2 ns in all instances.

S1.2.5 Fluorescence quantum yield of homosalate

The fluorescence quantum yield of HMS, Φ_{F}(HMS), was determined in all three solvents following the methodology described by Würth *et al.*,[8] by comparing the fluorescence emission to that of a known standard, 1,4-diphenyl-1,3-butadiene (DPB) in cyclohexane. All three solutions were prepared such that they had an absorbance value of 0.1 or below, which corresponds to a concentration of approximately 10 μM for HMS solutions and approximately 0.5 μM for the solution of DPB in cyclohexane. The UV-visible spectra of the sample and standard solutions are shown in Fig. S7a.

Five repeats of the emission spectra were taken for each of the fluorescence samples. These five emission spectra were averaged, and this average was used for the final calculation of Φ_{F}(HMS) using Eq. S5.[8] The averaged spectra are shown in Fig. S7b.

$$\Phi_{\mathrm{F}}^{x} = \frac{F_x A_s n_x^2}{F_s A_x n_s^2} \Phi_{\mathrm{F}}^{s} \tag{S5}$$

The parameters in Eq. S5 are defined as follows: Φ_{F}^{x} is the fluorescence quantum yield of the sample solution, Φ_{F}^{s} the fluorescence quantum yield of the standard, F_x is the integrated area of the fluorescence curves of the sample (320 – 600 nm), with F_s being the equivalent integral for the reference standard (320 – 600 nm); secondly A_s and A_x are the absorbance of the standard and sample respectively; finally n_s^2 is the refractive index of the solvent of the standard solution (cyclohexane) and n_x^2 is the refractive index of the sample solution. The value of Φ_{F}^{s} for these quantum yield calculations was 0.44.[9] However, as this value is for 330 nm excitation and fluorescence quantum yield is a wavelength dependent quantity, some caution should be exercised with the attained homosalate quantum yields.

S2 Supplementary results and discussion

S2.1 Gas-phase experiments discussion

S2.1.1 LIF linewidths

The first four peaks of the LIF spectrum of HMS were fitted with Lorentzian functions as shown in Fig. S10. As the LIF peaks are rotational band contours (the linewidths are those typical of a molecule the size of homosalate with rotational temperature of approximately 2 K), the Γ parameter in the Lorentzian fit gives an approximate lower bound to the lifetime of the vibrational level in S_1 by $\tau = \hbar/\Gamma$.[10] Following this analysis, the linewidth of the origin peak of HMS is ~ 0.84 cm^{-1}, which corresponds to a lifetime of the S_1-*enol* species of ~ 6 ps. We stress, however, that this is a lower limit value, which is reflected in the measured fluorescence lifetimes.

S2.2 Transient electronic absorption spectroscopy (TEAS) discussion

S2.2.1 Sequential fitting of homosalate

In the main manuscript, we have presented the results from fitting the TEAS data for HMS employing a parallel kinetic model, to allow for better comparison with the gas-phase data. To assess the effect of different model assumptions, we have also used a sequential model (that assumes $A \xrightarrow{\tau_1} B \xrightarrow{\tau_2} C \cdots \xrightarrow{\tau_4} E$) to fit the same data. The results of the sequential fitting are shown in Table S4. Selected wavelength transients to demonstrate the quality of the fit are shown in Fig. S13. These results demonstrate that the time constants extracted from fitting our TEAS data with a sequential model are similar to those yielded by a parallel kinetic model.

S2.2.2 TEAS measurements of ethylhexyl salicylate

TAS of ethylhexyl salicylate (EHS, also known as octisalate) were taken to compare the effects of the alkyl moiety on the action of the salicylate chromophore. The results are shown in Fig. S15, with TAS at selected pump-probe time delays in Fig. S16 and the quality of the fit shown for selected wavelengths in Fig. S17. The elucidated time constants, which were determined using the same methods as HMS, are listed in Table S5 for a parallel model and Table S6 for a sequential model.

As perhaps indicated by the similarities between the HMS and EHS in their UV-visible spectra (Fig. S15, see Fig. 1 in the main paper for equivalent spectra for HMS), there are comparable spectral features in the TAS for both of these molecules. The TAS for HMS can be found in Fig. 5 of the manuscript. Both sets of TAS share a prominent excited state absorption feature between *ca.* 320 – 400 nm, and a stimulated emission feature centred at 450 nm. Akin to HMS, four time constants were required to adequately fit the TAS obtained for EHS; the residuals for this fit are

shown in Fig. S12 (d), (e) and (f). The four time constants for EHS are comparable to those extracted for HMS, *i.e.* all four time constants are of the same orders of magnitude.

Given the similarities between HMS and EHS (and by comparison with previously published work), the extracted time constants can be confidently assigned to the same processes as were elucidated for HMS in the main paper. However, according to the results presented here, relaxation of EHS has been found to be relatively faster, perhaps indicating that the suggested internal conversion relaxation pathway from the S_1 state (plus any vibrational cooling that may take place alongside it, described by τ_2) may be facilitated by a molecular motion that is hindered by the larger or more rigid structure of the ester substituent in HMS when compared to EHS. Fluorescence, described by τ_3, was also found to have a slightly shorter decay lifetime for EHS when compared to HMS. As τ_1 is defined within the constraints of the IRF, any differences in the rate of intramolecular excited-state proton transfer for EHS *vs.* HMS are inconclusive. Similarly, it cannot be determined from our TEAS measurements whether the rate of intersystem crossing is affected, as for both HMS and EHS τ_4 is beyond the temporal window of the instrument.

In summary, whilst the photophysical processes occurring within HMS and EHS following photoexcitation in the UVB region may be the same in both molecules, suggesting that these processes are predominantly dictated by the salicylate chromophore, the alkyl chains of EHS as opposed to the cycloalkane structure of HMS may facilitate slightly faster rates of decay. From these results, it follows that EHS may be a preferential sunscreen candidate to HMS, given the reduction in the value of the fitted time constants.

S2.2.3 Longer-time scans

To further investigate any long-lived features in the TAS of both HMS and EHS, a second ultrafast transient absorption setup at the Warwick Centre for Ultrafast Spectroscopy was used; this setup was used as it has a longer delay stage and time delays of up to 3 ns could be accessed, as opposed to 2 ns. A full characterisation of this TEAS setup can be found in the publication by Woolley *et al.*,[3] although it is very similar to the setup used for all other TEAS studies in this work. For each time delay, 100 scans were taken and subsequently averaged. The pump wavelength was chosen to be the peak absorption (shown in Fig. 1) and the fluence of the pump and probe pulses was kept consistent between both setups for fair comparison. The results are shown in Fig. S18. These TAS demonstrate that there is a consistent positive long-lived feature in the TAS at probe wavelengths between *ca.* 360 – 480 nm, which is assigned to the T_1 state of HMS and EHS respectively. As mentioned in the main manuscript, the spectral features observed in these TAS resemble the triplet absorption spectra collected by Sugiyama *et al.*[11] for both HMS and EHS at room temperature (25 °C), 2–17 μs after photoexcitation, lending credibility to our hypothesis (see manuscript for further discussion).

S3 Supplementary figures

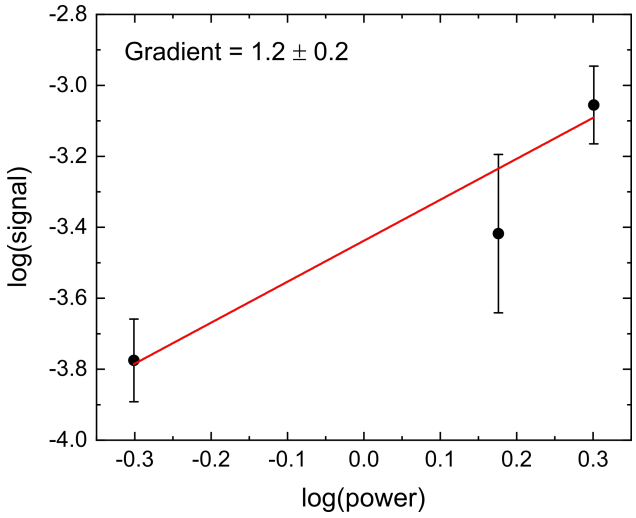

Fig. S1 Power dependence study for HMS in vacuum photoexcited at $\lambda_{\text{pump}} = 305$ nm at $\Delta t = 0$ ps. Black circles correspond to data points which are an average of four consecutive scans; the error bars on each data point correspond to two standard deviations from this average. The red line denotes the line of best fit attained by linear least squares regression.

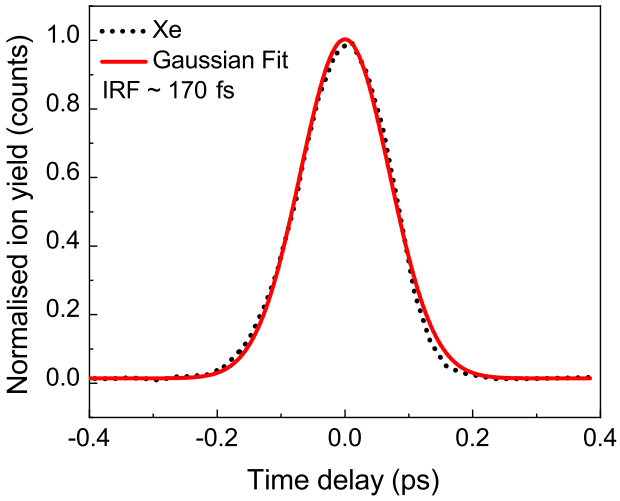

Fig. S2 Gaussian fit (red line) to the Xe TR-IY transients at $\lambda_{\text{pump}} = 330$ nm (black dotted line). The FWHM of the fitting curve presented provides us with the pump-probe beam cross-correlation width of ~ 170 fs, which we quote as our IRF.

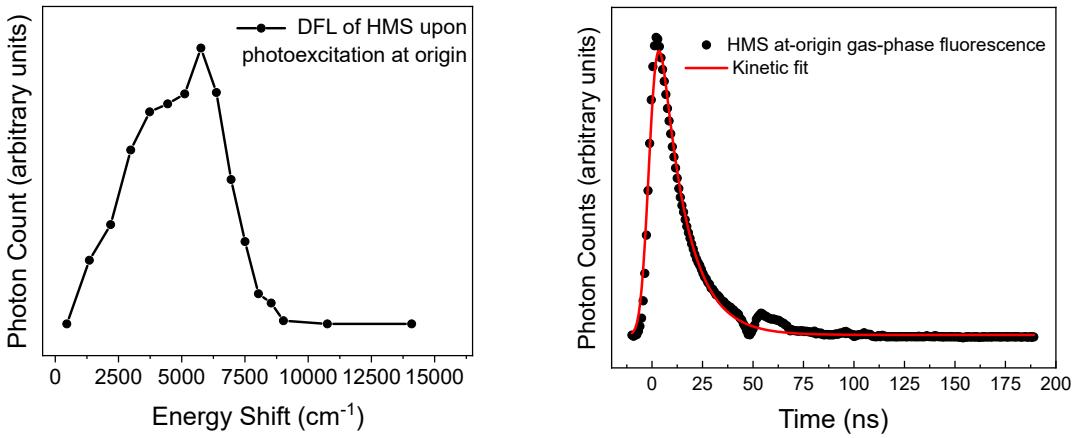

Fig. S3 (a) Dispersed fluorescence spectrum of HMS. (b) Fitted transient (black dotted line, with line of best fit shown in red) to extract the fluorescence lifetime of HMS at origin.

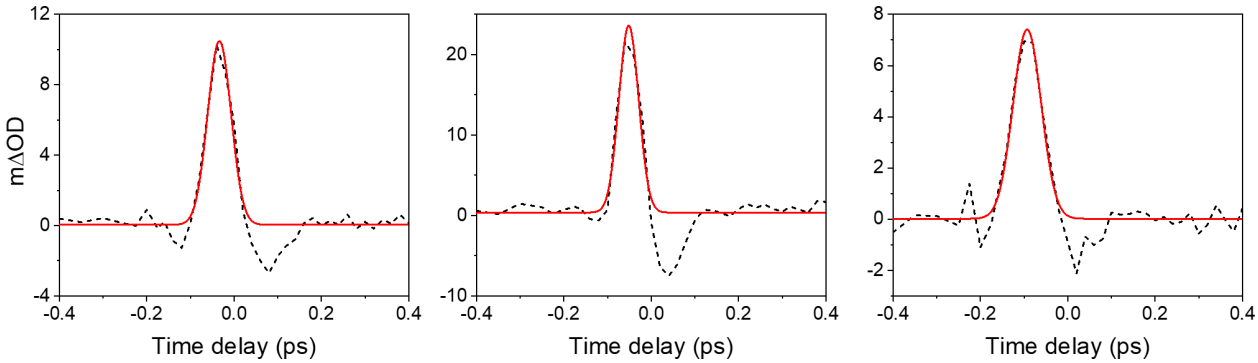

Fig. S4 Selected transients for solvent-only time-zero IRFs at given probe wavelengths, plotted using black dashed lines (pump wavelengths were kept the same as for TEAS measurements for each solution): (a) ethanol at 330 nm, IRF $\sim$ 65 fs (b) cyclohexane at 320 nm, IRF $\sim$ 55 fs and (c) acetonitrile at 330 nm, IRF $\sim$ 80 fs. These IRFs have been extracted from a Gaussian fit function, with the line of best fit shown in red.

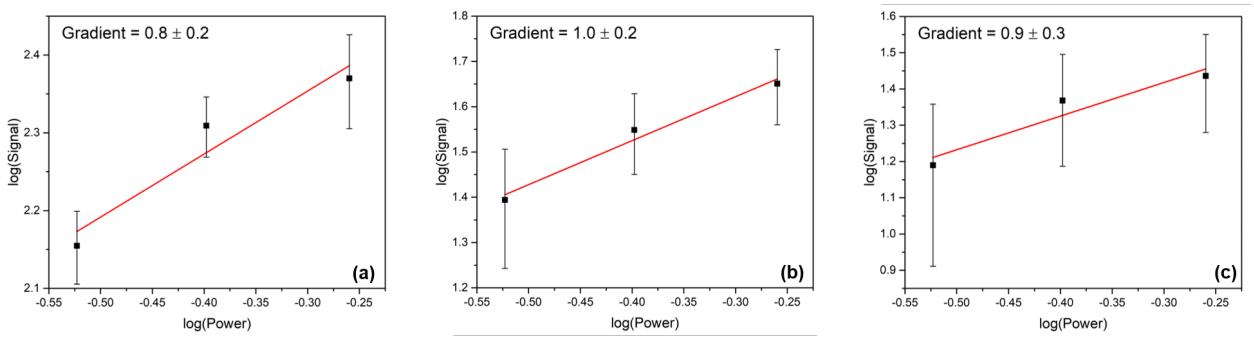

Fig. S5 Power dependency study for HMS in ethanol for key features at $\Delta t = 1$ ps at the following probe wavelengths: (a) 340 nm (b) 450 nm and (c) 530 nm. Explanation of the derivation of the error bars is given in the text in Section S1.2.3.

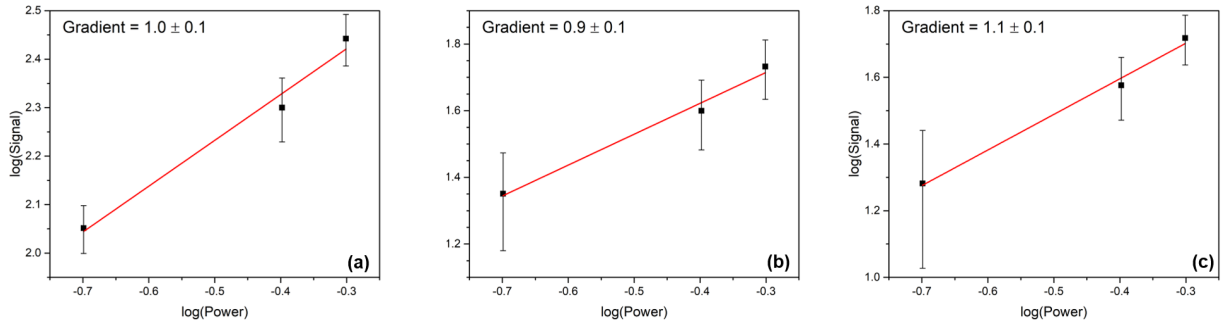

Fig. S6 Power dependency study for ethylhexyl salicylate (octisalate) in ethanol for key features at $\Delta t = 1$ ps at the following probe wavelengths: (a) 340 nm (b) 450 nm and (c) 530 nm. Explanation of the derivation of the error bars is given in the text in Section S1.2.3.

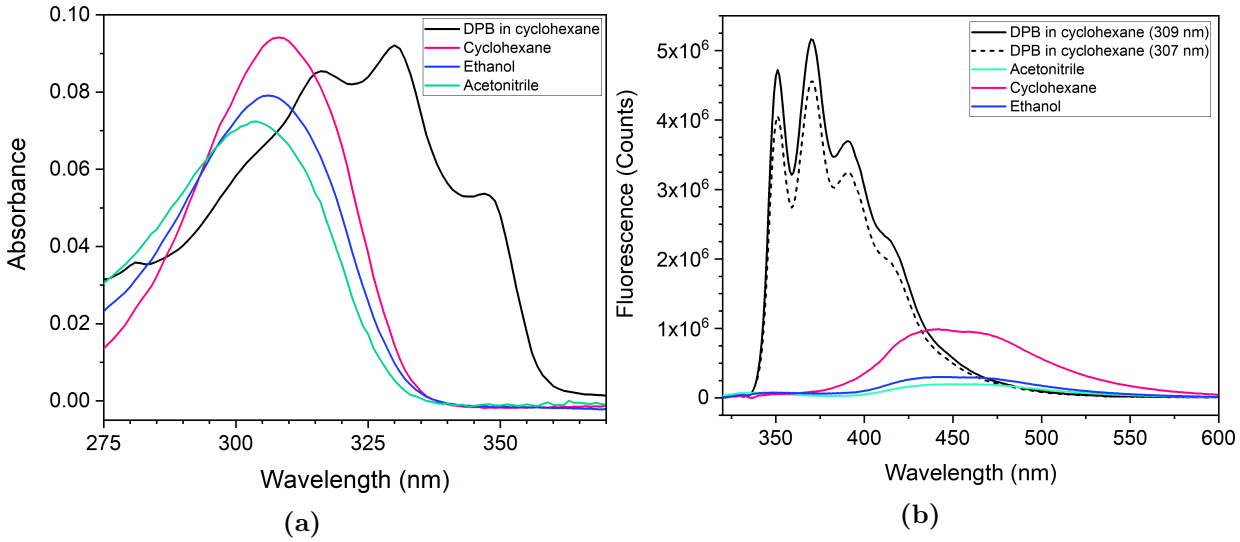

Fig. S7 (a) UV-visible spectra taken of three $\sim$ 20 μM solutions of HMS in cyclohexane (pink line), ethanol (blue line) and acetonitrile (green line), with the standard solution, $\sim$ 0.5 μM 1,4-diphenyl-1,3-butadiene (DPB) in cyclohexane, shown in black. (b) Averaged fluorescence spectra, attained from averaging five separate scans, which were integrated and the values substituted into Eq. S5.

Conformer	Relaxed S_0	Relaxed S_1
Conformer 1	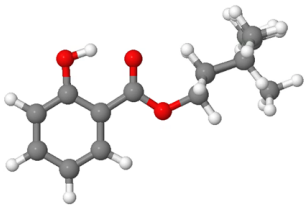 0 eV	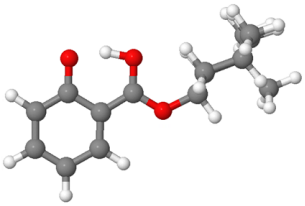 3.90 eV
Conformer 2	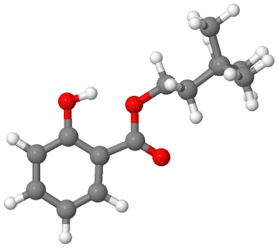 0.17 eV	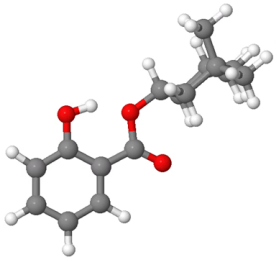 4.30 eV

Fig. S8 Structure and relative energies (relative to conformer 1 in the S_0 state, the lowest energy structure/state) of the two lowest energy conformers of HMS in both the S_0 and S_1 states. The ground state energies were calculated by relaxing the geometry of both conformers at the PBE/cc-pVTZ level of theory and then conducting a single point energy calculation on each at the PBE0/cc-pVTZ level of theory. The excited state energies were calculated by relaxing each conformer with respect to the S_1 state at the PBE0/cc-pVTZ level of theory.

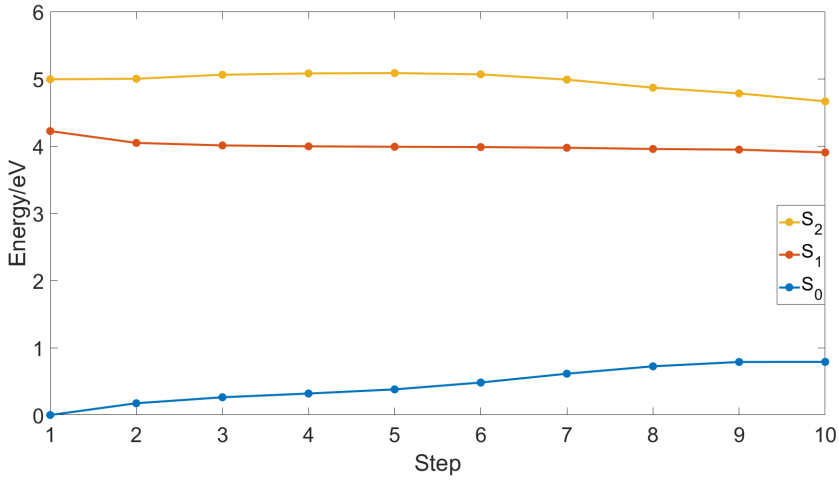

Fig. S9 S_0, S_1, and S_2 energies of HMS in specific steps between the *enol* and *keto* forms. These steps were generated through a linear interpolation of internal coordinates (LIIC). This figure is an expansion upon Fig. 2b in the main text to demonstrate the lack of intersection between the S_1 and S_2 states over the examined reaction coordinate. As the second conformer does not yield a stable *keto* structure in the S_1 state, it is not possible to study a LIIC along its respective proton transfer coordinate.

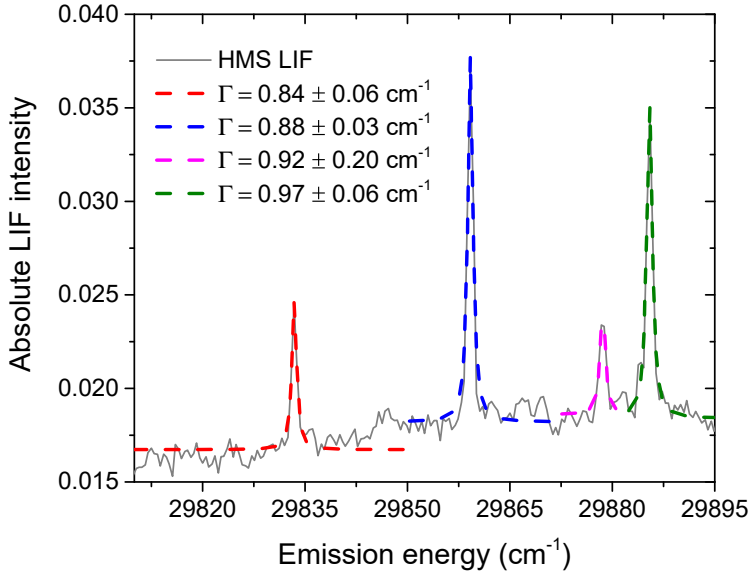

Fig. S10 Lorentzian fits (dashed lines) to the first four peaks of the LIF spectrum of HMS (raw data presented as a grey solid line). These Lorentzian fits return Γ values of 0.84 cm^{-1} for the peak centred at 29833.4 cm^{-1} ($S_1(v = 0)$ origin of HMS, red dashed line), 0.88 cm^{-1} for the peak at 29859.2 cm^{-1} (blue dashed line), 0.92 cm^{-1} for the peak at 29878.6 cm^{-1} (pink dashed line) and 0.97 cm^{-1} for the peak at 29885.5 cm^{-1} (green dashed line).

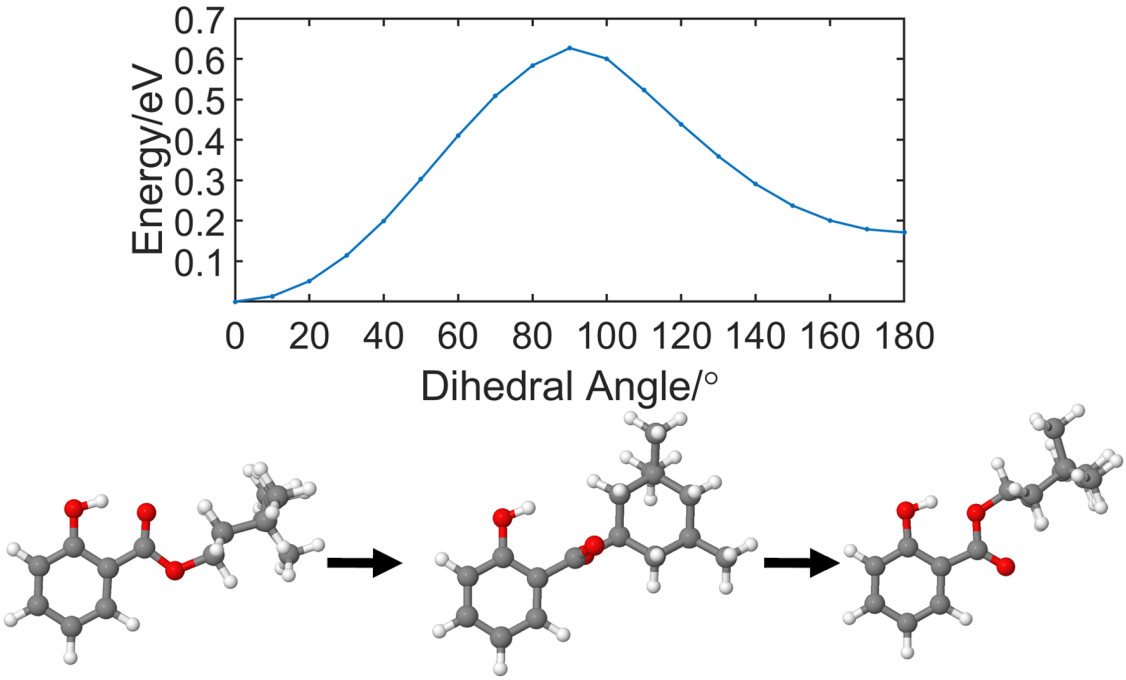

Fig. S11 S_0 energy of *enol* form along the rotation coordinate between conformer 1 and conformer 2. This was generated by fixing the dihedral angle shown at 10 degree increments between 0 and 180 degrees and relaxing all other internal coordinates in the ground state at the PBE/cc-pVTZ level of theory. This is an upper bound to the energy barrier between the two conformers.

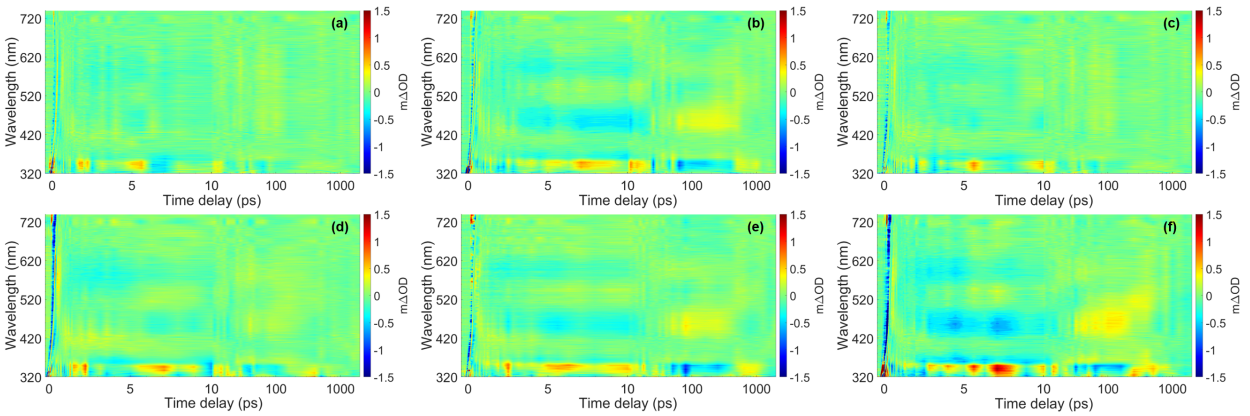

Fig. S12 False colour heat maps showing the residuals attained from the parallel fitting procedure (compared to raw data) for HMS in (a) acetonitrile, (b) cyclohexane and (c) ethanol, and for EHS in (d) acetonitrile, (e) cyclohexane and (f) ethanol

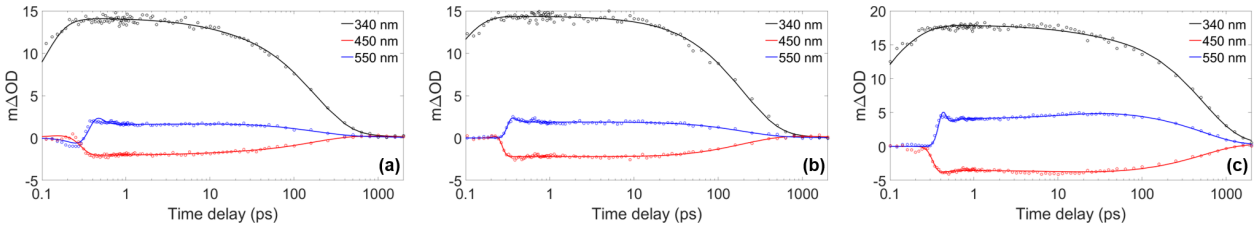

Fig. S13 Kinetic fits of the transient data at 340 nm (black), 450 nm (red) and 550 nm (blue) for HMS in (a) acetonitrile, (b) ethanol and (c) cyclohexane. The circles represent the raw data and the solid line is the fit attained using the sequential model described in Section S2.2.1.

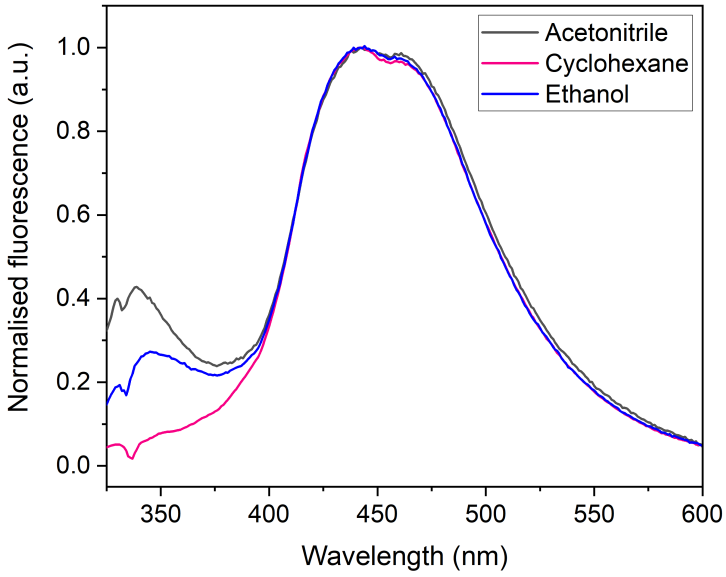

Fig. S14 Normalised emission spectra with solvent baseline subtraction of HMS in cyclohexane, ethanol and acetonitrile. Excitation was carried out at the respective peak maxima of each solution: $305 \leq \lambda_{\text{pump}} \leq 310$ nm. The slit width was 2.5 nm. The slight discrepancy in the spectra at $\sim$ 330 nm is due to Stokes Raman scattering effects that could not be fully subtracted from the fluorescence spectra.[1] All three solutions display an emission peak at 450 nm. We note, however, the presence of a smaller peak at 350 nm in polar solvents, a phenomenon that has also been observed in the molecular analogue methyl salicylate, although the cause of this dual fluorescence remains uncertain.[2]

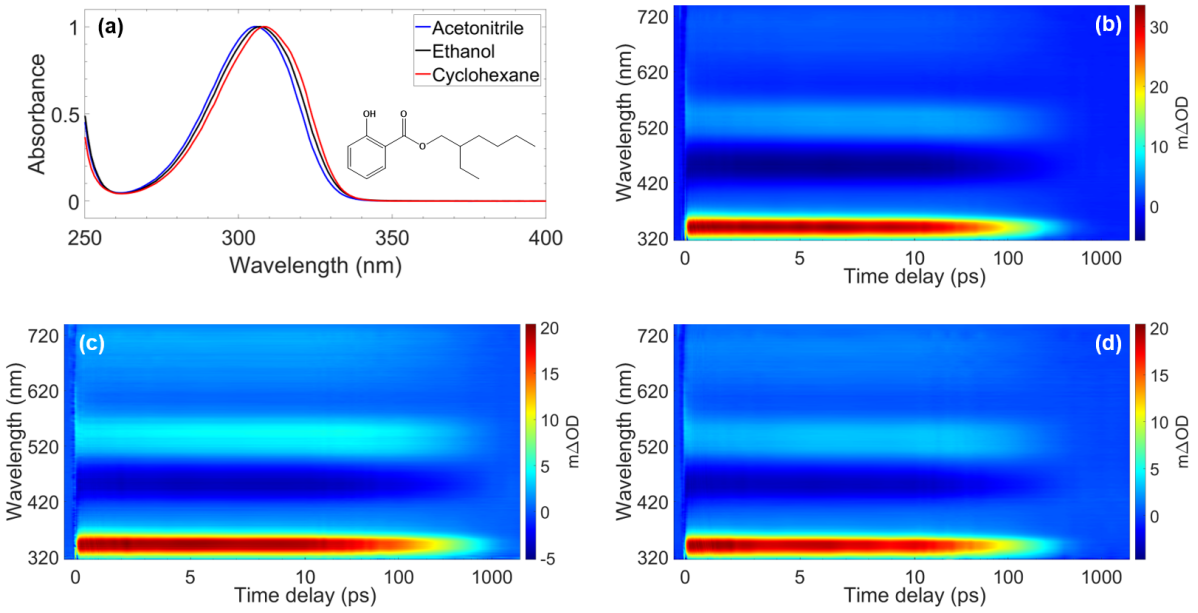

Fig. S15 (a) UV-visible absorption spectra of EHS in three different solvents, with the molecular structure of EHS inset. TAS of $\sim$ 10 mM solutions of EHS in (b) ethanol (λ_{max} = 307 nm), (c) cyclohexane (λ_{max} = 309 nm) and (d) acetonitrile (λ_{max} = 305 nm).

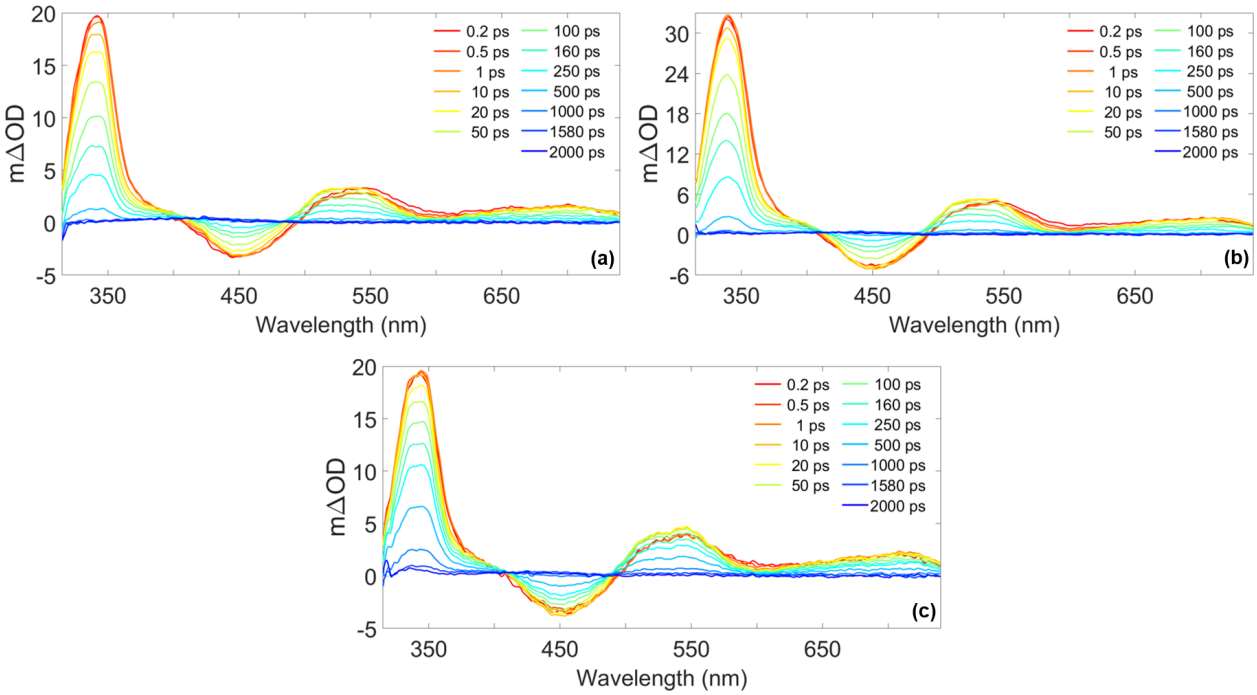

Fig. S16 TAS at selected pump-probe time delays for EHS in (a) acetonitrile, (b) ethanol and (c) cyclohexane. These plots are attained by taking vertical slices through the false colour heat maps at the given time delay.

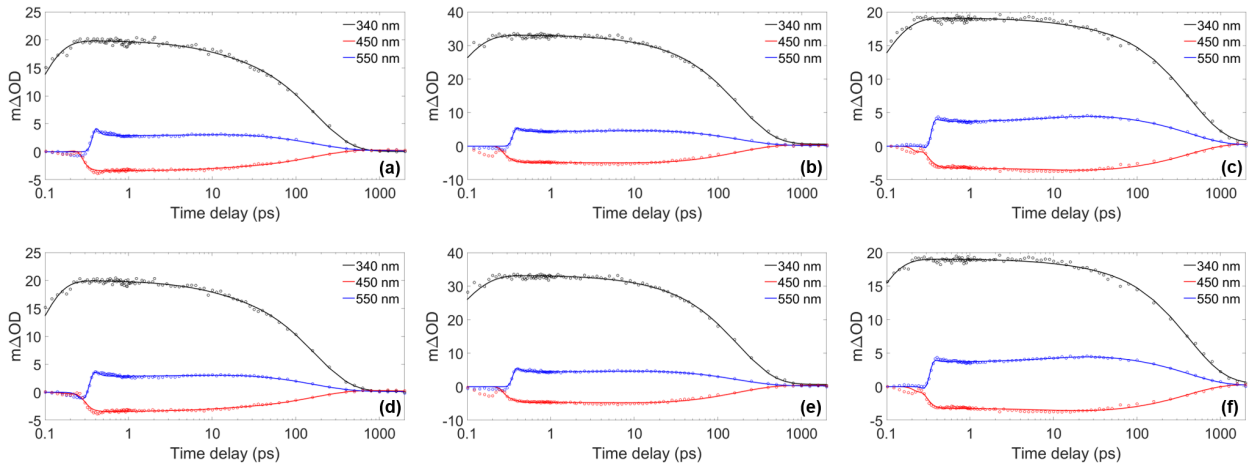

Fig. S17 Kinetic fits of the transient data at 340 nm (black), 450 nm (red) and 550 nm (blue) for EHS in acetonitrile, ethanol and cyclohexane respectively, fitted using: (a)–(c) a parallel model, the same as that used for HMS (described in the manuscript) and (d)–(f) a sequential model, as described in section S2.2.1. The circles denote the raw data at each wavelength and the solid line is the fit attained. In each case, the time delay axis is presented on a logarithmic scale.

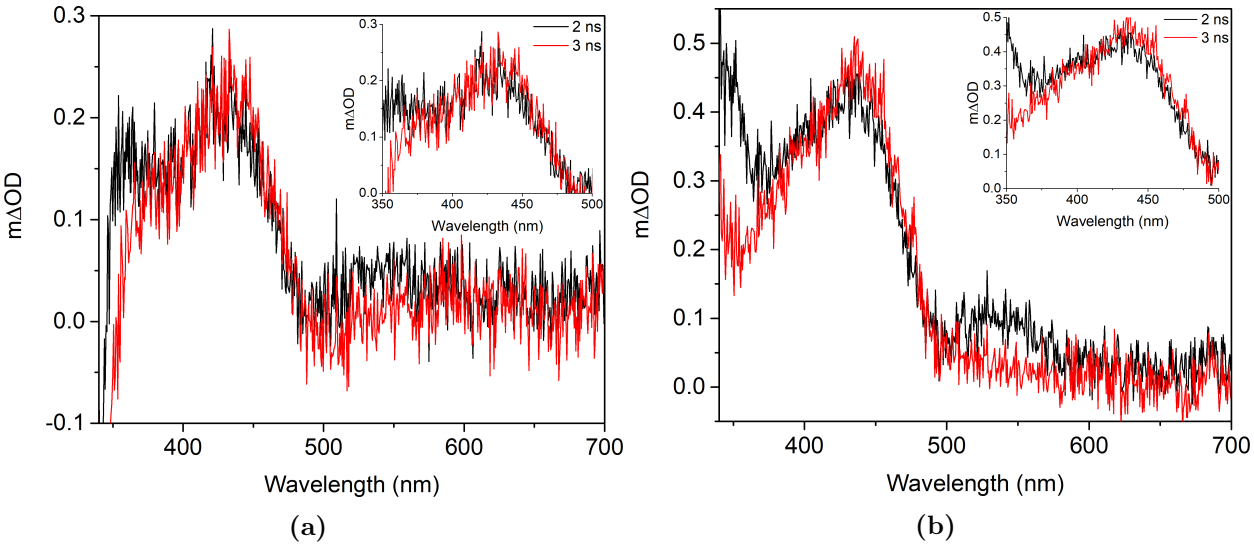

Fig. S18 (a) TAS of HMS in cyclohexane ($\lambda_{\text{pump}} = 309$ nm) taken at $\Delta t = 2$ ns (black) and $\Delta t = 3$ ns (red), attained using the TEAS setup characterised by Woolley *et al.*[3] Inset is a zoom-in of the data between 350 and 500 nm to more clearly display the long-lived positive signal. (b) TAS of EHS in cyclohexane ($\lambda_{\text{pump}} = 309$ nm) taken at $\Delta t = 2$ ns (black) and $\Delta t = 3$ ns (red). Inset is a zoom-in of the data between 350 and 500 nm to more clearly display the long-lived positive signal.

S4 Supplementary tables

Table S1 This table shows the difference in energies of conformer 1 and conformer 2 ($E_2 - E_1$) in the gas-phase. Both conformers were relaxed at the PBE/cc-pVTZ level of theory. Following this, the single point energies of these structures were calculated using PBE/cc-pVTZ and PBE0/cc-pVTZ, as well as the post Hartree-Fock method MP2/cc-pVDZ.

Level of Theory	$E_2 - E_1$
PBE/cc-pVTZ	0.17 eV
PBE0/cc-pVTZ	0.17 eV
MP2/cc-pVDZ	0.10 eV

Table S2 Calculated singlet and triplet excited state vertical energies from the optimised ground state geometry of the *enol* form of HMS in cyclohexane using TD-DFT at the PBE0/cc-pvtz level of theory

Environment	**Singlets**			**Triplets**		
	State	Energy (eV)	Character	State	Energy (eV)	Character
Vacuum				ΔT_1	3.3282	
	S_1	4.2220	$\pi\pi^*$	T_1	3.2149	$\pi\pi^*$
	S_2	4.9928	$n\pi^*$	T_2	3.4260	$\pi\pi^*$
	S_3	5.3280	$\pi\pi^*$	T_3	3.2714	$\pi\pi^*$
	S_4	6.0780	$\pi\pi^*$	T_4	4.6214	$n\pi^*$
	S_5	6.9246	$n\pi^*$	T_5	5.1866	$n\pi^*$
Acetonitrile				ΔT_1	3.3490	
	S_1	4.2917	$\pi\pi^*$	T_1	3.2749	$\pi\pi^*$
	S_2	4.9808	$n\pi^*$	T_2	3.4721	$\pi\pi^*$
	S_3	5.3383	$\pi\pi^*$	T_3	4.2983	$\pi\pi^*$
	S_4	5.9317	$n\pi^*$	T_4	4.6229	$n\pi^*$
	S_5	6.0869	$n\pi^*$	T_5	5.1041	$n\pi^*$
Cyclohexane				ΔT_1	3.3364	
	S_1	4.2518	$\pi\pi^*$	T_1	3.2423	$\pi\pi^*$
	S_2	4.9826	$n\pi^*$	T_2	3.4447	$\pi\pi^*$
	S_3	5.3341	$\pi\pi^*$	T_3	4.2825	$\pi\pi^*$
	S_4	6.0381	$n\pi^*$	T_4	4.6167	$n\pi^*$
	S_5	6.2335	$n\pi^*$	T_5	5.1490	$n\pi^*$
Ethanol				ΔT_1	3.3334	
	S_1	4.2914	$\pi\pi^*$	T_1	3.2724	$\pi\pi^*$
	S_2	5.0225	$n\pi^*$	T_2	3.4700	$\pi\pi^*$
	S_3	5.3222	$\pi\pi^*$	T_3	4.2990	$\pi\pi^*$
	S_4	5.9212	$n\pi^*$	T_4	4.6685	$n\pi^*$
	S_5	6.0698	$n\pi^*$	T_5	5.1444	$n\pi^*$

Table S3 Calculated singlet and triplet excited state vertical energies from the optimised ground state geometry of the *keto* form of HMS in cyclohexane using TD-DFT at the PBE0/cc-pvtz level of theory.

Environment	**Singlets**			**Triplets**		
	State	Energy (eV)	Character	State	Energy (eV)	Character
Vacuum				ΔT_1	2.1752	
	S_1	3.1149	$\pi\pi^*$	T_1	1.9677	$\pi\pi^*$
	S_2	3.8748	$n\pi^*$	T_2	3.2909	$\pi\pi^*$
	S_3	4.9279	$\pi\pi^*$	T_3	3.6810	$n\pi^*$
	S_4	5.5817	$\pi\pi^*$	T_4	3.9888	$\pi\pi^*$
	S_5	5.9169	$\sigma\pi^*$	T_5	4.9728	$\pi\pi^*$
Acetonitrile				ΔT_1	2.1748	
	S_1	3.1638	$\pi\pi^*$	T_1	2.0821	$\pi\pi^*$
	S_2	3.8806	$n\pi^*$	T_2	3.2680	$\pi\pi^*$
	S_3	4.9272	$\pi\pi^*$	T_3	3.7012	$n\pi^*$
	S_4	5.4921	$n\pi^*$	T_4	3.9675	$\pi\pi^*$
	S_5	5.5897	$\pi\pi^*$	T_5	5.0146	$\pi\pi^*$
Cyclohexane				ΔT_1	2.1592	
	S_1	3.1254	$\pi\pi^*$	T_1	1.9980	$\pi\pi^*$
	S_2	3.8506	$n\pi^*$	T_2	3.2811	$\pi\pi^*$
	S_3	4.9257	$\pi\pi^*$	T_3	3.6629	$n\pi^*$
	S_4	5.5521	$\pi\pi^*$	T_4	3.9756	$\pi\pi^*$
	S_5	5.8401	$n\pi^*$	T_5	4.9805	$\pi\pi^*$
Ethanol				ΔT_1	2.2286	
	S_1	3.2289	$\pi\pi^*$	T_1	2.1780	$\pi\pi^*$
	S_2	4.0426	$n\pi^*$	T_2	3.2718	$\pi\pi^*$
	S_3	4.9389	$\pi\pi^*$	T_3	3.8665	$n\pi^*$
	S_4	5.5077	$n\pi^*$	T_4	3.9875	$\pi\pi^*$
	S_5	5.6220	$\pi\pi^*$	T_5	5.0896	$\pi\pi^*$

Table S4 Extracted transient electronic absorption spectroscopy time constants for HMS solutions upon photoexcitation at λ_{max}, obtained via global fitting techniques using a sequential model.[4] Whilst the error for τ_1 is given by half the instrument response in each solvent (Fig. S4), the errors presented for τ_2 to τ_4 are those provided by the fitting software package; the quality of the fits can be gauged from the corresponding residuals (Fig. S12) and kinetic fits (Fig. S13).

Time constant	Ethanol	Cyclohexane	Acetonitrile
τ_1 (fs)	55 ± 35	105 ± 30	80 ± 40
τ_2 (ps)	10.4 ± 0.4	14.2 ± 0.5	9.1 ± 0.4
τ_3 (ps)	199 ± 2	533 ± 6	176 ± 2
τ_4 (ns)	$> 2^*$	$> 2^*$	$> 2^*$

* Outside the temporal window of the instrument (2 ns).

Table S5 Extracted transient electronic absorption spectroscopy time constants for EHS solutions upon photoexcitation at λ_{max}, obtained via global fitting techniques using a parallel model.[4] Whilst the error for τ_1 is given by half the instrument response in each solvent (Fig. S4), the errors presented for τ_2 to τ_4 are those provided by the fitting software package; the quality of the fits can be gauged from the corresponding residuals (Fig. S12) and kinetic fits (Fig. S17).

Time constant	Ethanol	Cyclohexane	Acetonitrile
τ_1 (fs)	65 ± 35	50 ± 30	50 ± 40
τ_2 (ps)	8.8 ± 0.4	10.8 ± 0.3	9.3 ± 0.3
τ_3 (ps)	176 ± 2	412 ± 4	169 ± 2
τ_4 (ns)	$> 2^*$	$> 2^*$	$> 2^*$

* Outside the temporal window of the instrument (2 ns).

Table S6 Extracted transient electronic absorption spectroscopy time constants for EHS solutions upon photoexcitation at λ_{max}, obtained via global fitting techniques using a sequential model.[4] Whilst the error for τ_1 is given by half the instrument response in each solvent (Fig. S4), the errors presented for τ_2 to τ_4 are those provided by the fitting software package; the quality of the fits can be gauged from the corresponding kinetic fits (Fig. S17).

Time constant	Ethanol	Cyclohexane	Acetonitrile
τ_1 (fs)	60 ± 35	65 ± 30	50 ± 40
τ_2 (ps)	9.0 ± 0.3	10.9 ± 0.3	9.6 ± 0.4
τ_3 (ps)	176 ± 2	422 ± 4	170 ± 2
τ_4 (ns)	$> 2^*$	$> 2^*$	$> 2^*$

* Outside the temporal window of the instrument (2 ns).

References

[1] R. J. Clarke and A. Oprysa, *Journal of Chemical Education*, 2004, **81**, 705.

[2] F. Ling, D. Liu, S. Li, W. Li, B. Zhang and P. Wang, *The Journal of Chemical Physics*, 2019, **151**, 094302.

[3] J. M. Woolley, M. Staniforth, M. D. Horbury, G. W. Richings, M. Wills and V. G. Stavros, *The Journal of Physical Chemistry Letters*, 2018, **9**, 3043–3048.

[4] J. Snellenburg, S. Laptenok, R. Seger, K. Mullen and I. Van Stokkum, *Journal of Statistical Software*, 2012, **49**, 1–22.

[5] J. L. Rodgers and W. A. Nicewander, *The American Statistician*, 1988, **42**, 59–66.

[6] I. Walmsley, L. Waxer and C. Dorrer, *Review of Scientific Instruments*, 2001, **72**, 1–29.

[7] M. P. Grubb, A. J. Orr-Ewing and M. N. R. Ashfold, *Review of Scientific Instruments*, 2014, **85**, 064104.

[8] C. Würth, M. Grabolle, J. Pauli, M. Spieles and U. Resch-Genger, *Nature Protocols*, 2013, **8**, 1535–1550.

[9] B. Hudson and B. Kohler, *Annual Review of Physical Chemistry*, 1974, **25**, 437–460.

[10] Y. Chiang, P. V. Demekhin, A. I. Kuleff, S. Scheit and L. S. Cederbaum, *Physical Review A*, 2010, **81**, 032511.

[11] K. Sugiyama, T. Tsuchiya, A. Kikuchi and M. Yagi, *Photochemical & Photobiological Sciences*, 2015, **14**, 1651–1659.